Molecular Photovoltaics and Surface Potentials at the Air−Water Interface

Ida Lee,[†,‡] Brian L. Justus,[§] James W. Lee,[‡] and Elias Greenbaum*[,‡,||]

Department of Electrical and Computer Engineering, University of Tennessee, Knoxville, Tennessee 37996, Chemical Sciences Division, Oak Ridge National Laboratory, Oak Ridge, Tennessee 37831, Optical Sciences Division, Naval Research Laboratory, Washington, DC 20375, and Genome Science & Technology Program and Center for Environmental Biotechnology, University of Tennessee, Knoxville, Tennessee 37996

Received: August 24, 2003; In Final Form: October 8, 2003

An experimental approach that directly measures light-induced electrostatic surface potentials at the gas−liquid interface using the combined techniques of the atomic force microscope and the scanning surface-potential microscope is presented. Photosystem I (PSI) reaction centers, one of the molecular photovoltaic structures of green plants, convert light energy into electrical energy. We report the orientation and measurement of light-induced photovoltages at the air−water interface by PSI solutions entrained in the pores of microchannel glass. The data indicate that illuminated PSI reaction centers reversed the sign of the water surface electrostatic potential from negative to positive and that additional illumination further increased the positive value of the potential. The sign of the light-induced photopotentials indicates that the reaction centers are oriented with their electron-transport vectors pointing toward the water phase. Electrostatic potentials as a function of PSI concentration are presented for concentrations of active PSI up to 1 μM. Orienting biomolecules at the air−water interface might be an enabling technology for new classes of sensors.

Introduction

A defining feature of nanoscale bioscience and biotechnology is extraction of functional single biomolecules and in vitro reconstitution on patterned surfaces or in defined geometries. Photosynthesis, the biological process of solar-energy absorption by green plants and subsequent conversion of light energy for plant growth, uses two nanometer-scale molecular reaction centers operating in series, Photosystems I (PSI) and II. The first step of the conversion process is absorption of photons in the reaction centers. The absorbed energy triggers vectorial electron-transfer reactions that generate voltages across the reaction center complexes. It is these voltages and their associated electrochemical potentials that are the sources of Gibbs energy that drives the energetically uphill reactions of photosynthesis.[1] It has been shown by direct measurement of the open- and closed-circuit electric potentials that purified PSI reaction centers retain their full photovoltaic properties.[2,3] It is demonstrated in this paper that the pores of microchannel glass can be used to immobilize columns of liquid for study of the electrostatic potentials of interfacial photoactive biomolecules. Surface-potential distributions provide a new analytical method to characterize electrostatic features of single molecules and the dynamic forces that act at this interface. We report quantitative light-induced electrostatic measurements of PSI reaction centers using atomic force microscope (AFM)[4] and the scanning surface-potential microscope (SSPM).[5] By use of the combined AFM/SSPM technique, absolute orientation of the photon-activated electron-transport vector can be deduced from the sign of the photovoltages. Moreover, the small pore size of microchannel glass is an ideal sample holder and delivery system for microcantilever sensing of molecules at the gas−water interface. The presence of illuminated PSI reaction centers at the gas−water interface has a dramatic effect on the sign and magnitude of the interfacial surface potentials. The results indicate that our approach may be useful for characterizing the interfacial properties of micro/nano fluidic systems for molecular process analysis, environmental monitoring, clinical diagnostics, drug discovery, cell culture, cell manipulations, protein analysis, PCR, DNA sizing and sequencing, etc.

Materials and Methods

Microchannel glass with hollow channels arranged in a 2-D hexagonal close-packed array was used as the substrate. The key advantage in using microchannel glass is that it minimizes liquid movement so that the SSPM technique can be used. The microchannel glass substrate was ∼400 μm thick; the diameter of the channels was 5−6 μm. Fabrication of the channel glass has been previously described.[6] Briefly, the porous substrates were etched wafers of microchannel plate glass. Microchannel glass boules, ∼25 cm in length and 3 cm in diameter, were purchased from Litton EOS (Garland, TX). The glass had hexagonal close-packed, acid-etchable elements that were ∼5.5 μm in diameter. The center−center pitch between the acid-etchable elements was ∼8 μm. The boule was cut into wafers, ranging in thickness from 0.25 to 2 mm, using a diamond saw, and both surfaces of the wafers were ground and polished. The microstructured region of the polished wafers was ∼27 mm from flat to flat. The surface area of the microstructured region was about 5 cm^2, and the channel density was $>10^6$/cm^2. The wafers were annealed at 500 °C for 1 h before they were etched in 1% (by volume) acetic acid solution. The etched wafers were rinsed with deionized water. The resulting microchannel glass substrates contained hollow channels that were uniformly circular,

* Author to whom correspondence may be addressed. E-mail: greenbaum@ornl.gov.

[†] Department of Electrical and Computer Engineering, University of Tennessee.

[‡] Oak Ridge National Laboratory.

[§] Naval Research Laboratory.

[||] Genome Science & Technology Program and Center for Environmental Biotechnology, University of Tennessee.

10.1021/jp036518h CCC: $25.00
Published on Web 11/27/2003

perpendicular to the surface, and parallel to one another. The special properties of microchannel glass enable detailed study of liquid samples at the gas−liquid interface by presenting liquid samples that are compatible with scanning microprobe techniques. That is to say, the defined geometry of the microchannels combined with an easily recognizable difference between the glass and liquid permit the study of a static liquid surface in an isolated environment. This is an ideal technique for the study of molecules at the gas−liquid interface.

Distilled water prepared from an high-performance liquid chromatography-grade Barnsted Nanopure II System was used for the experiments. Double-distilled water was used for preparation of the PSI buffer solution. Nanopure water or aqueous PSI solutions were drawn into the microchannels from the bottom of the microchannel plate by capillary action. The liquid-infiltrated microchannel glass was then anchored on a metal plate for AFM and SSPM measurements. The measurements were performed in ultrapure nitrogen gas at 30−40% relative humidity. Exclusion of atmospheric oxygen eliminated the known slow oxidation of the P700/P700$^+$ couple. The humidity was adjusted to maintain a constant liquid volume during the course of the experiments. The liquid level inside the microchannel glass substrate was determined by monitoring laser light reflected from the liquid surface with a microscope and CCD camera. It is known that water droplets shrink and eventually evaporate when the relative humidity is less than 25%, while droplet growth occurs when the humidity is greater than 60%.[7] It is also known that, on average, capillary forces have their largest contributions to microscale adhesive interactions at a relative humidity of 50%.[8]

PSI reaction center−core antenna complexes containing about 40 chlorophylls per photoactive P700 (PSI-40) were isolated from spinach thylakoids using detergent (Triton X-100) solubilization and hydroxyapatite column purification.[9] PSI was eluted in a buffer that contained 0.2 M phosphate (pH 7.0) and 0.05% Triton X-100 in double-distilled water. For the six-month storage stability data, PSI was diluted to eight different concentrations starting with a 1.06 μM stock solution, whereas for the one-month data, the starting solution was 0.85 μM. The characteristics of both one- and six-month-old PSI solutions were confirmed by absorption spectroscopy (maxima at 440 and 672 nm) and by P700 oxidation kinetic spectroscopy in the presence of 20 mM sodium ascorbate and 0.5 mM methyl viologen. P700 oxidation measurements were performed with a Walz spectrometer that measured the kinetic profile of the light-induced differential absorption between 810 and 860 nm. In the presence of sodium ascorbate, the reduction kinetics of P700$^+$ are biphasic, 24 s^{-1} for reduction by F_{AB}^- and 0.1 s^{-1} by ascorbate.

A modified Nanoscope IIIa (Digital Instruments) was used to study the surface potentials. First, the surface topography was measured by recording a linear trace with AFM operating in tapping mode. By use of the built-in lift-mode feature, the surface topography trace was followed immediately by a second, spatially elevated, trace for measurement of the electric potential at a set height of 30 nm above the sample surface. The surface topography and the corresponding SSPM map were recorded on a raster-by-raster basis with alternating sequential scans at a scan rate of 1 Hz; 265 lines were used to form two-dimensional images. Two sources of light illuminated the PSI. One was an external diode laser (670 nm, 3.98 mW) that could be turned on and off. The second laser light source (1.1 mW) comprised part of the optical technique used for cantilever measurement. It was intrinsic to the measuring technique and caused multiple reflections within the microchannel plate. Therefore, it was not possible to obtain a true dark value for surface potentials in the presence of PSI. The surface potential in the presence of PSI was measured under background illumination plus additional illumination from the external laser. The AFM/SSPM head was enclosed in a chamber with humidity and gas control.

The SSPM was calibrated with specially prepared surface structures in which gold was sputtered on ultraflat cover-glass slides. Various dc step voltages provided by a constant voltage source were correlated with the electric-potential image map of the structures obtained with SSPM. The calibration data indicated a minimum detection limit of 1 mV. As described previously,[2] a long and slender but slightly blunt SSPM probe was used. With this probe design (apex radius of 100 nm), the measured potential is approximately equal to the actual potential (error $\leq$ 5%).[10]

Results and Discussion

Figure 1A illustrates the AFM topography of a microchannel glass substrate with Nanopure water inside each channel. Figure 1B is the corresponding SSPM image of the electrostatic surface potential. The electrostatic potential above the water surface at the center of each microchannel is slightly negative. This result suggests that a net number of water molecules at the air−water interface is oriented with their oxygen atoms pointing toward air and both OH bonds pointing inward to the bulk water. As presented in Figure 1B, surface defects and irregularities caused measurement artifacts near the periphery of the microchannels. Therefore, we did not attempt to construct electrostatic-potential maps over the entire water surface. The observation of a slightly negative water surface potential is consistent with previous analysis.[11] As indicated by ref 11, large differences exist between the magnitudes of the experimental potential measurements and theoretical calculations. By use of the sum frequency generation (SFG) technique, Du and co-workers determined that ~20% of the surface water molecules have one free OH bond that is directed out of the surface while the other OH bond points into the bulk liquid.[12,13] This orientation contributes to a positive water surface potential. Subsequent theoretical analysis, using an ab initio molecular dynamics simulation, suggested that the dipole angle is 110° relative to the surface normal for surface water molecules with one dangling OH pointing toward the vapor. The negative contribution to the surface potential comes from the majority (~80%) of the dipoles at the interface that are oriented at about 120° with both OH arms pointing inward toward the bulk water.[14,15] This gives pure water a net negative electrostatic surface potential. Figure 2A illustrates the AFM surface topographic image of a microchannel plate with a buffered PSI solution entrained in each channel. Figure 2B is the corresponding SSPM electrostatic surface-potential image. A diode laser (670 nm) plus background light illuminated the gas−PSI solution interface during the measurement. The sign of the electrostatic potential above the PSI solution was opposite to that measured above the pure water surface.

The finite size of the cantilever and microchannel create a measurement artifact in electric potential near the rim of the channel. The artifact is illustrated in parts A and B of Figure 1 by the arrows. This surface potential artifact arises from the shape of the AFM/SSPM probe and the limitations imposed by the vertical sample geometry. Figure 3 schematically illustrates that the actual trajectory of the AFM probe does not faithfully trace the vertical wall of the glass channel due to the tip shape and the electronics (feedback and gain). Instead, the probe follows the vertical step as a steep slope (square dotted line). The lift mode deployed for the SSPM measurement (long-dashed

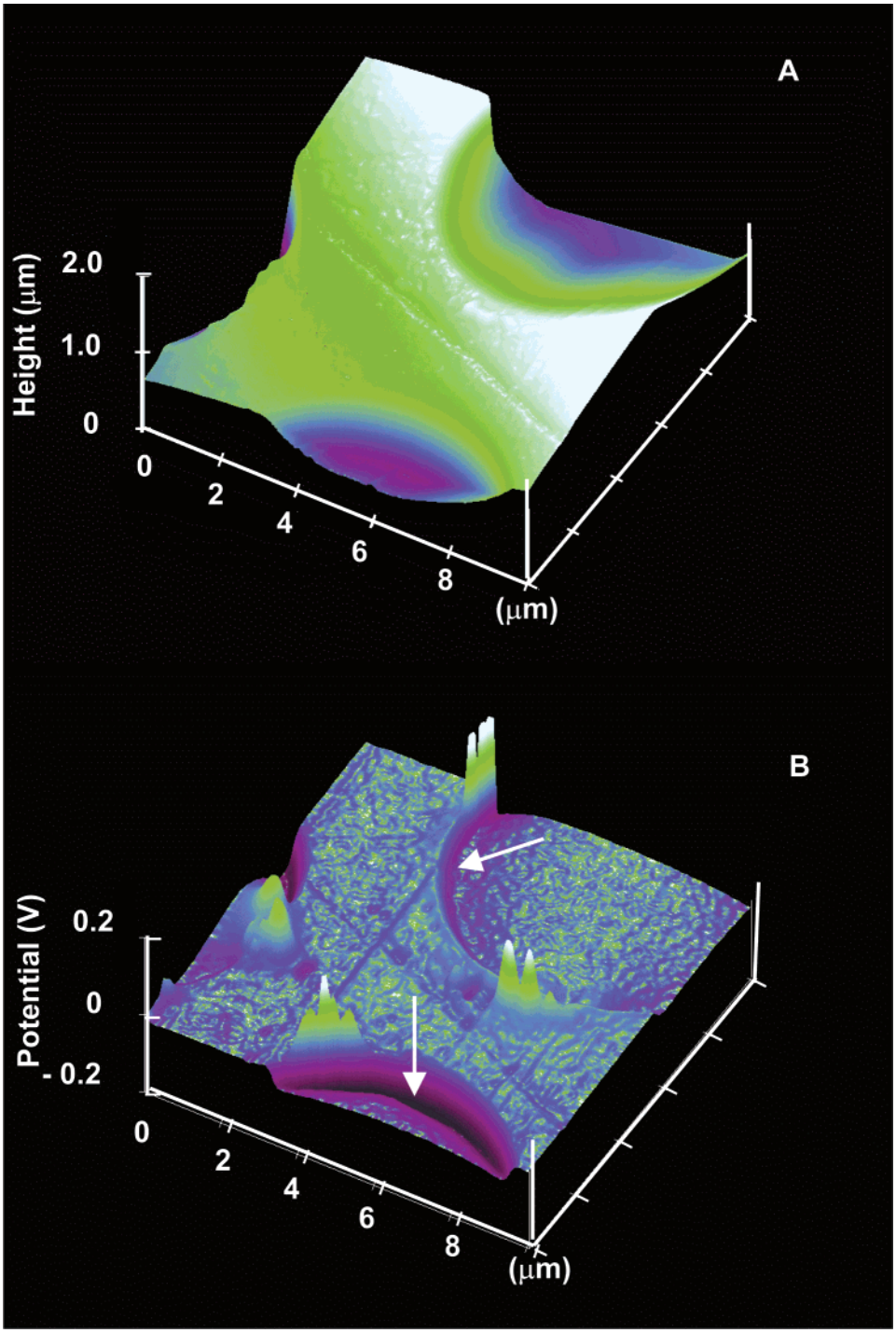

Figure 1. (A) AFM topographic image of the microchannel plate with Nanopure water in each channel. (B) The corresponding SSPM potential measurement of part A. The arrows indicate the rim artifact caused by the finite size of the cantilever and microchannel. Please see text for additional details.

line) elevates the tip above the sample to a height "a" above the sample surface relative to the AFM trace. In the central region of the channel, the electrostatic potentials measured by the SSPM probe are those "a" nm above the sample. However, near the edge it is considerably elevated above the surface ("c" in Figure 3) and in close proximity to the glass wall ("b" in Figure 3). It can be seen by inspection of Figure 3 that the SSPM measurement near the edge is a conflation of one the of two forces, one from the side wall of the channel and the other from the liquid. We have not attempted to deconvolute the respective contributions of the two forces. In any event, the data measured close to the edge should not be thought of as a signal from either substrate or liquid. We have also observed strong potential contrasts at the rim that showed positive spikes around the edge in Figure 1B and Figure 2B. This is probably due to small particles or sharp protrusions of different materials and high charge density at the periphery of the channels. For similar reasons, exaggeration of the surface potential has been observed for particles equal in size or smaller than the scanning probe,[16] thus enabling the use of SSPM for examining the uniformity of thin-film deposition on substrates.[17] Surface potential is also very sensitive to surface chemical composition because the potential depends on the dielectric properties of the adsorbent on the sample surface.[18,19] During the polishing of the channel glass, particles of different materials may have adsorbed at the

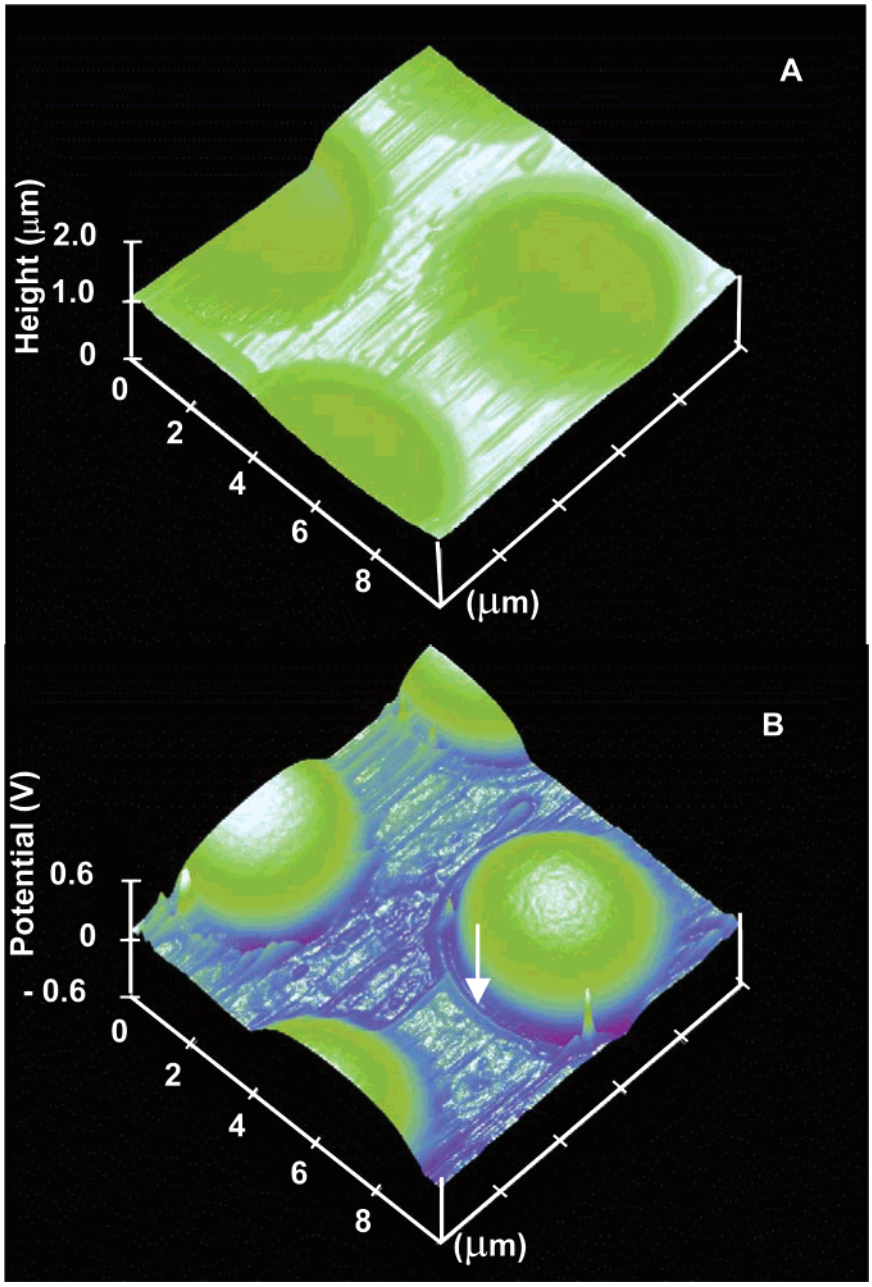

Figure 2. (A) AFM topographic image of the microchannel plate with PSI solution inside each microchannel. (B) The corresponding SSPM potential measurement of part A. The channels were illuminated with light from the SSPM cantilever-detection system and an external diode laser. The arrow indicates the edge-effect artifact.

channel's rim and produced the strong surface-potential enhancement observed in the SSPM image.

Therefore, to avoid edge-effect artifacts, we measured the value of the surface potential at a fixed location above a channel's central region (>2 μm from the edge) as a function of time instead of AFM/SSPM scanning of the entire channel area. For data acquisition, the zero vertical position of the probe was first established on the glass substrate. It was then lifted 30 nm, and the electrostatic potential of the glass substrate was measured as a function of time. The substrate was then moved laterally such that the cantilever was positioned above the central region of a microchannel well. The zero vertical position of the probe was re-established at the liquid surface, the probe was again lifted 30 nm as before, and the surface potential of the liquid was measured versus time. Figure 4 A illustrates the surface potential of the glass substrate (at ground potential) and surface potential of the water vs time. The surface potential of water in the middle of a microchannel, averaged over 30 s, is -30 ± 2 mV. A similar method has been used by others to measure the surface potential of water adsorbed on a mica surface at a relative humidity between 40 and 80%.[20] It was found that a water film on mica is at least 0.4 V more negative than that under dry conditions. This potential is more negative than that measured above the microchannel well surface because on the muscovite mica {001} surface, a much greater degree of water dipole orientation occurs. Both molecular dynamics simulations[21] and SFG results[22] showed that no free OH dangling bonds are present in the saturated single ice-like bilayer, so that the dipole moments of the water molecules point toward the mica, while the negative oxygen end is exposed. In our measurements of the potential of free-water surfaces, both SFG and molecular dynamics simulation[12,13] have shown that ~20−25% of the water molecules at the liquid−vapor interface are oriented with the dangling hydrogen pointing outward and

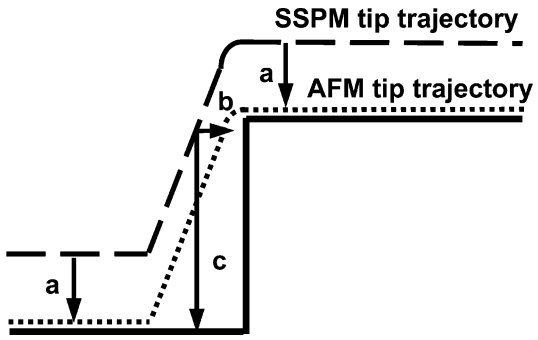

Figure 3. Schematic illustration of cantilever trajectories. The vertical step of the microchannel rim is drawn as a solid line. The AFM trace is illustrated as a square dotted line. Note steep slope at the step instead of a vertical drop. The SSPM lift mode (long-dashed line) lifts the tip to height "a" above the sample surface relative to the AFM trace. The potentials measured by SSPM are "a" nm above the aqueous surface except near the rim where the relevant distances are "c" and "b" as defined in the figure.

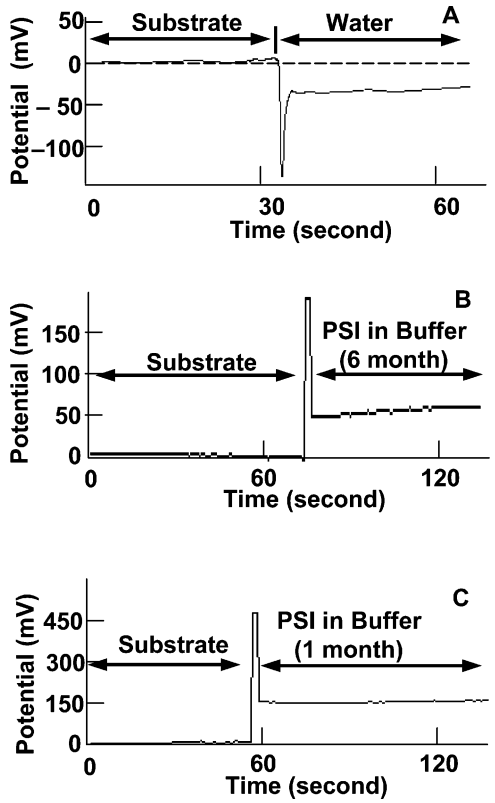

Figure 4. (A) The surface potential of a centrally located fixed point above the glass substrate and water in a microchannel as a function of time; similar measurements for a (B) six- and (C) one-month-old PSI solution stored at 4 °C. The sample was laterally positioned for measurement above the glass or an aqueous microchannel. For SSPM measurements with pure buffer, please see the inset to Figure 5. Pure buffer causes a surface potential of 3.3 mV. There is no difference in activity between fresh and one-month-old PSI.

the rest of the water molecules (~75−80%) with the negative oxygen end exposed.[14,15] The presence of both positive and negative ends of the water dipole at the free-water surface implies partial dipole moment cancellation, leaving the net negative component that we measured. The kinetic profiles of P700+ steady-state formation and reduction were the same for both six- and one-month-old PSI solutions, but significant differences were observed in the potential measurements by SSPM.

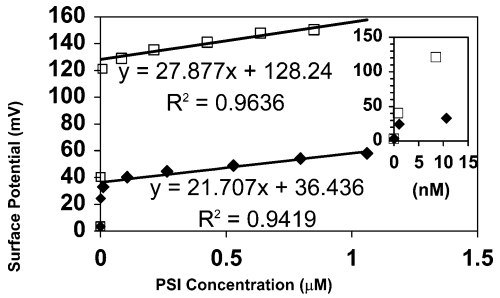

Figure 5. Surface potentials for pure buffer and PSI as a function of concentration. Data points are presented for six-month-old (◆) and one-month-old (□) samples stored at 4 °C. The inset expands the low concentration data.

Figure 4B illustrates the potential above a PSI solution that was stored at 4 °C for about six months as a function of time. The average surface potential during a 60-s interval was +58 mV relative to the substrate. Figure 4C is a similar experiment for a PSI solution that was less than one month old and is essentially the same as a newly prepared sample. In this case, the average surface potential for 60 s was +150 mV compared with the substrate. The potential above each solution was measured under the combined illumination of an external diode laser plus background illumination of the optical detection system. The surface potentials of the PSI solutions are typically ~20 mV more positive when the external diode laser is on, suggesting that the electron-transport vector of the PSI reaction center points to the bulk water phase. As discussed above, even when the external diode laser was off, the channels still experienced considerable illumination from the internal laser that was used to monitor both the cantilever amplitude and liquid levels in the other channels. This light can reach the channels by undergoing scattering and multiple reflections inside the glass substrate. Because of the optics that are an integral part of our measuring system and the high degree of multiple scattering within and between the glass microchannels, this technique does not permit a light-minus-dark measurement of the photoinduced voltages. Black microchannel glass is presently unavailable.

Figure 5 shows the surface potentials of PSI solutions for both the one- and six-month-old PSI solutions as a function of concentration. Eight different concentrations ranging from 0 (buffer only) to ~1 μM were used. Surface potentials in the low concentration range (0−10 nM) are illustrated in the inset. We observed a linear relationship between PSI concentration and surface potential in the range 0.1−1.0 μM for both the one- and six-month-old samples. By use of an elementary exponential model for decay, we can use linear regression equations and the data of Figure 5 to obtain an approximate estimate of the lifetime for PSI stored at 4 °C. The potentials measured for the two samples are 156 and 58 mV. Assuming a first-order exponential decay for PSI photoactivity and that the surface potential is proportional to the concentration of chemically active PSI, we can use the one- and six-month-old potentials to calculate the decay rate of PSI using the equation

$$C_A(t) = C_A(0)e^{-kt} \quad (1)$$

where C_A is the concentration of photochemically active PSI and t is the decay time measured in months. The calculated decay rate, k, is 0.165 month^{-1}. Equation 1 predicts that after approximately four months storage at 4 °C, half the PSI in the solution remains photochemically active. The loss of activity is most likely due to bacterial growth. Bacteria usually multiply exponentially.

Conclusions

We report topographic and electrostatic measurements of the air−water and air−PSI solution interface in channels of microchannel glass using AFM/SSPM techniques. By laterally positioning the substrate and sample, we measured surface potentials above water and PSI solutions for one- and six-month-old samples. On the basis of the photovoltaic measurements, we estimated the rate of PSI activity decay for storage at 4 °C. Our results indicate that surface dipole forces and orientation of water molecules causes a net interfacial orientation of PSI molecules and light-induced surface potential that is related to the PSI concentration and photoactivity. The results also suggest that the electron-transport vector of the PSI reaction center points toward the water.

Acknowledgment. The authors thank M. S. Humayun and J. Weiland for helpful advice and discussions on the potential biomedical applications of microchannel glass and B. Mathis for secretarial support. This research was supported by the Department of Energy Offices of Basic Energy Sciences and Biological and Environmental Research and the National Science Foundation via a subcontract with the Doheny Eye Institute. Support was also provided by the Office of Naval Research and the Oak Ridge National Laboratory Director's R&D Fund. Oak Ridge National Laboratory is managed and operated by UT-Battelle, LLC, for the U.S. Department of Energy under contract DE-AC05-00OR22725.

References and Notes

(1) Blankenship, R. E. In *Molecular Mechanisms of Photosynthesis*; Blackwell: Williston, VT, 2002.

(2) Lee, I.; Lee, J. W.; Stubna, A.; Greenbaum, E. *J. Phys. Chem. B* **2000**, *104*, 2439−2443.

(3) Millsaps, J. F.; Bruce, B. D.; Lee, J. W.; Greenbaum, E. *Photochem. Photobiol*. **2001**, *73*, 630−635.

(4) Binnig, G.; Quate, C. F.; Gerber, C. *Phys. Rev. Lett.* **1986**, *56*, 930−933.

(5) Fujihara, M.; Kawate, H.; Yasutake, M. *Chem. Lett.* **1992**, 2223−2226.

(6) Tonucci, R. J.; Justus, B. L.; Campillo, A. J.; Ford, C. E. *Science* **1992**, *258*, 783−785.

(7) Masuda, H. *Material Trans., JIM* **1999**, *40*, 169−181.

(8) Ouyang, Q.; Ishida, K.; Okada, K. *Appl. Surf. Sci.* **2001**, *169*, 644−648.

(9) Owens, T. G.; Webb, S. P.; Mets, L.; Alberte, R. S.; Fleming, G. R. *Proc. Natl. Acad. Sci. U. S. A* **1987**, *84*, 1532−1536.

(10) Jacobs, H. O.; Leuchtmann, P.; Homan, O. J.; Stemmer, A. *J. Appl. Phys.* **1998**, *84*, 1168−1173.

(11) Paluch, M. *Adv. Colloid Interface Sci.* **2000**, *84*, 27−45.

(12) Du, Q.; Superfine, R.; Freysz, E.; Shen, Y. R. *Phys. Rev. Lett.* **1993**, *70*, 2313−2316.

(13) Du, Q.; Freysz, E.; Shen, Y. R. *Science* **1994**, *264*, 826−828.

(14) Morita, A.; Hynes, J. T. *Chem. Phys.* **2000**, *258*, 371−390.

(15) Vassilev, P.; Hartnig, C.; Koper, M. T. M.; Frechard, F.; van Santen, R. A. *J. Chem. Phys.* **2001**, *115*, 9815−9820.

(16) Yamashina, S.; Shigeno, M. *J. Electron Microsc*. **1995**, *44*, 462−466.

(17) Shiraishi, S.; Kanamura, K.; Takehara, Z. *J. Phys. Chem. B* **2001**, *105*, 123−143.

(18) Fujihira, M.; Kawate, H. *Thin Solid Films* **1994**, *243*, 163−169.

(19) Chi, L. F.; Jacobi, S.; Fuchs, H. *Thin Solid Films* **1996**, *284−285*, 403−407.

(20) Bluhm, H.; Inoue, T.; Salmeron, M. *Surf. Sci*. **2000**, *462*, L599-L602.

(21) Odelius, M.; Bernasconi, M.; Parrinello, M. *Phys. Rev. Lett.* **1997**, *78*, 2855−2858.

(22) Miranda, P. B.; Xu, L.; Shen, Y. R.; Salmeron, M. *Phys. Rev. Lett*. **1998**, *81*, 5876−5879.